Available online at www.sciencedirect.com
SCIENCE DIRECT
ELSEVIER
Journal of the European Ceramic Society 26 (2006) 95–109
ECERS
www.elsevier.com/locate/jeurceramsoc

Fatigue crack growth in ferroelectrics under electrical loading

Jay Shieh[a], John E. Huber[b,*], Norman A. Fleck[b]

[a] *Department of Materials Science and Engineering, National Taiwan University, 1 Roosevelt Road, Sec. 4, Taipei, Taiwan*
[b] *Department of Engineering, University of Cambridge, Trumpington Street, Cambridge CB2 1PZ, UK*

Received 8 August 2004; received in revised form 12 October 2004; accepted 16 October 2004
Available online 8 December 2004

Abstract

Fatigue crack growth is investigated in the polycrystalline ferroelectrics PZT-5H and PLZT 8/65/35 under electrical loading. The fatigue cracks exhibit features such as bifurcation and tunnelling, followed by crack arrest. The nature of the resulting damage differs in the two materials: in PZT-5H a narrow zone of intergranular cracks propagates across the specimen, wedging the crack surfaces apart. In PLZT 8/65/35 a broad microcracked band spreads across the specimen. The rate of crack growth is found to correlate well with the amplitude of electric displacement.

Keywords: Electroceramics; Ferroelectricity; Fatigue; PZT; PLZT

1. Introduction

Ferroelectric ceramics experience fatigue cracking under the influence of alternating electric fields, which degrades their electrical and mechanical properties and thus reduces their reliability. The growth in applications of ferroelectrics as electromechanical sensors, electronic filters, micropositioners and displacement actuators[1,2] has made fatigue a critical issue faced by manufacturers of ferroelectric components.

In the ferroelectrics literature, the term *fatigue* generally refers to the gradual degradation of bulk material properties, such as the saturation remanent polarization, in a cyclically loaded specimen. Most studies in this area have focused on the electrical degradation of ferroelectrics, i.e. the cycle dependence of remanent polarization, strain hysteresis, coercive field and dielectric constant of ferroelectric ceramics upon electrical fatiguing.[18–26] In contrast, the present experimental study is concerned with the distinct phenomenon of fatigue cracking—the nucleation and growth of cracks or microcrack damage due to cyclic electrical loading.

In several previous experimental studies of electric field-induced fatigue crack growth of ferroelectric ceramics, researchers have grown fatigue cracks from Vicker's indentations, and have shown that the predominant direction of fatigue crack growth is perpendicular to the applied electric field.[3–5] The phenomenon of fatigue crack growth in ferroelectrics under cyclic electric fields above the coercive field (E_c) is well documented.[4,6] Electric field-induced fatigue crack growth in PZT under an alternating electric field below the coercive field has also been observed.[7] Weitzing et al.[8] explored fatigue cracking in three different PZT materials (one rhombohedral composition and two morphotropic compositions with different grain sizes) under cyclic electric fields up to $1.5E_c$; they found that the fatigue crack growth rate decreases with increasing cycle number, and a saturation point is reached after approximately 10^5 cycles. Several authors have used in situ field-emission scanning electron microscopy (SEM) and transmission electron microscopy (TEM) to study crack tip deformation and microcracking from fine pores due to electrical loading.[9–11] By altering the relative orientation between the poling and electrical loading directions, it has been demonstrated that an indentation crack could be redirected to propagate on planes which are inclined to the original crack plane.[12,13]

* Corresponding author. Tel.: +44 1223 332781; fax: +44 1223 332662.
E-mail address: naf1@eng.cam.ac.uk (J.E. Huber).

0955-2219/$ – see front matter © 2004 Elsevier Ltd. All rights reserved.
doi:10.1016/j.jeurceramsoc.2004.10.002

A substantial literature now exists concerning electric field induced fatigue crack growth. However, there is still a lack of agreement on the fundamental mechanism. Cao and Evans[6] presented a crack wedging mechanism which explains steady-state electric field-induced fatigue crack growth as a result of the actuation of asperities along the fracture surfaces, giving active wedging. Zhu and Yang[14–17] argued that the non-uniform domain switching near the crack tip leads to strain mismatches and produces a cyclic stress field characterised by a cyclically varying stress intensity factor near the crack tip. There is a lack of data for fatigue crack growth over 10^6 or more cycles; moreover, the available data are limited in scope in terms of material type, and loading amplitude.

The current study gives a systematic set of measurements of fatigue crack growth in ferroelectrics under purely electrical loading and assesses various possible correlating parameters. Some of the fatigue crack growth data have been previously presented;[27] the present work extends and develops this previous study by reporting additional measurements, detailed morphology of fatigue cracks, and by calculating each of a set of loading parameters in order to find a parameter that correlates with the rate of crack growth. The correlating parameters considered are the range of electric field, ΔE; the range of applied voltage, ΔV; the range of electric displacement, ΔD; the cyclic J-integral, ΔJ and the cyclic dissipation, ΔW. The evaluation of ΔJ from readily available experimental measurements is discussed in Section 2. The focus of the experimental part of this study in Sections 3 and 4 is on the characterisation and observed mechanism of crack propagation in two ferroelectric compositions: soft lead zirconate titanate (PZT-5H) and lanthanum-doped lead zirconate titanate (PLZT) of composition La/Zr/Ti = 8/65/35. Electric field-induced fatigue crack growth measurements, in the form of crack extension as a function of the number of cycles, are presented. The dielectric hysteresis of cracked specimens of the two materials during fatigue, and the morphology of the fatigue crack itself, are described. Critical information required for the evaluation of potential correlating parameters is obtained from the experimental data.

2. Evaluation of ΔJ

Consider a non-linear ferroelectric solid in which the state of stress σ_{ij}, electric field E_i, strain ε_{ij} and electric displacement D_i are known at each material point. Assume the existence of the electric enthalpy h defined by

$$h = h(\varepsilon_{ij}, D_i) = \int \sigma_{ij}\,\mathrm{d}\varepsilon_{ij} - \int E_i\,\mathrm{d}D_i \tag{1}$$

The J-integral is defined on a closed path Γ with unit outward normal n_i that surrounds a crack tip C in the solid, as shown in Fig. 1a. In a linear piezoelectric solid, the integral

$$J = \int_\Gamma (hn_1 - \sigma_{ij}n_j u_{i,1} + D_j n_j E_1)\,\mathrm{d}\Gamma \tag{2}$$

is path independent and is equal to the energy release rate G for a crack parallel to the x_1 direction, propagating in the x_1 direction.[28] Care is needed in evaluating J because closure of the path within the body requires the path to include a portion of the crack faces. There is an electrical contribution to J from the crack surface when $D_j n_j E_1$ is non-zero. However, under some circumstances the contribution to Eq. (2) from $D_j n_j E_1$ vanishes on the crack surface. The "impermeable" crack model assumes a charge free crack surface and a crack medium with zero permittivity; in this case, $D_j n_j = 0$ everywhere on the crack surface and hence the contribution from $D_j n_j E_1$ vanishes. Similarly, in a conducting crack, $E_1 = 0$, and again $D_j n_j E_1$ vanishes.

The concept of a cyclic J-integral, ΔJ has been used to characterise fatigue crack growth where bulk yielding occurs.[29] Let the minimum load point in a fatigue cycle correspond to loading $(\boldsymbol{\sigma}^0, \boldsymbol{E}^0)$ and a strain and electric displacement state of $(\boldsymbol{\varepsilon}^0, \boldsymbol{D}^0)$. Define deviations from the minimum load state during the loading part of the cycle by $\Delta\boldsymbol{\sigma} = \boldsymbol{\sigma} - \boldsymbol{\sigma}^0$ and so forth. A cyclic J-integral can be defined by

$$\Delta J = \int_\Gamma (h^{\mathrm{c}} n_1 - \Delta\sigma_{ij} n_j \Delta u_{i,1} + \Delta D_j n_j \Delta E_1)\,\mathrm{d}\Gamma \tag{3}$$

where h^{c} is a cyclic analogue of the electric enthalpy, defined by

$$h^{\mathrm{c}} = \int \Delta\sigma_{ij} d\Delta\varepsilon_{ij} - \int \Delta D_i d\Delta E_i \tag{4}$$

In the present work, the electrical fatigue of a rectangular specimen with a thin crack growing parallel to the surface electrodes is considered (see Fig. 1b). The specimen has zero traction on its surface, and zero voltage along BC, while a voltage V is applied along the surface ED. For the integration contour ABCDEFGA of Fig. 1b, the cyclic J-integral becomes

$$\Delta J = \int_{\mathrm{AB+CD+EF}} h^{\mathrm{c}} n_1\,\mathrm{d}\Gamma + \int_{\mathrm{FGA}} D_j n_j \Delta E_1\,\mathrm{d}\Gamma \tag{5}$$

In writing Eq. (5), terms $h^{\mathrm{c}} n_1$ vanish along FGA because n_1 vanishes on the surface of a thin crack. Also, the approximation $D_i n_i E_1 = 0$ is made along the external surface ABCDEF of the specimen. This is justified on BC and DE because the presence of conducting electrodes ensures that $E_1 = 0$. On AB, CD and EF the external medium has a much smaller permittivity than that of the specimen, and the surfaces carry no free charge, such that $D_i n_i \sim 0$. If the crack is thin and conductive, then the contribution to ΔJ from segment FGA vanishes, giving

$$\Delta J = \int_{\mathrm{AB+CD+EF}} h^{\mathrm{c}} n_1\,\mathrm{d}\Gamma \tag{6}$$

Eq. (6) allows ΔJ to be evaluated as the net flux of electric enthalpy into the specimen during the loading part of the cycle. The assumption of a conductive crack may in practice be more realistic than the assumption of an impermeable crack,

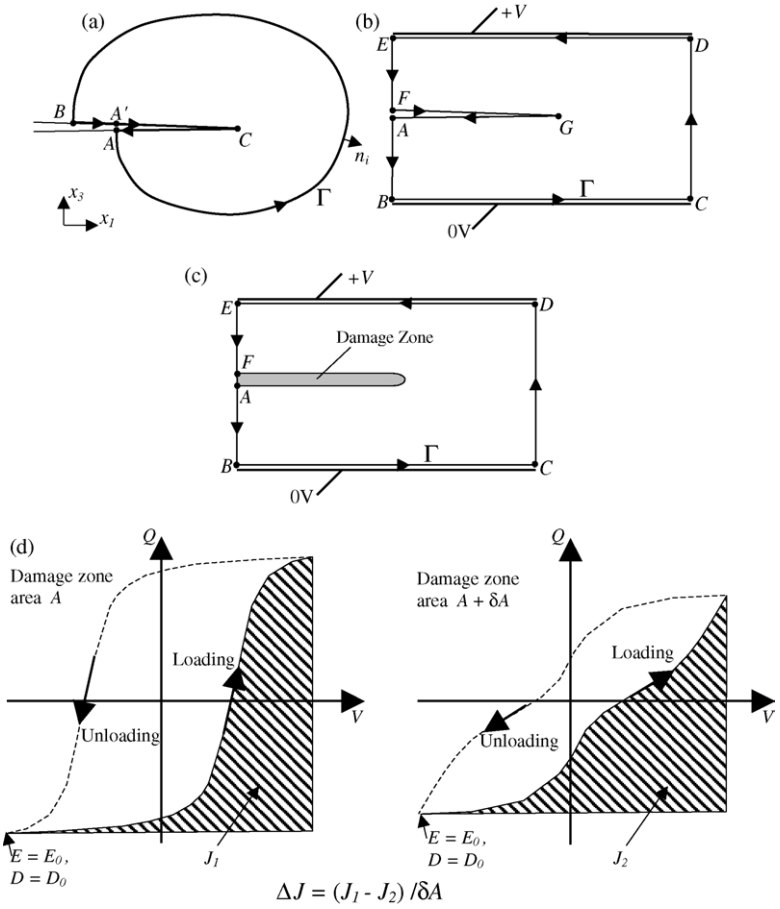

Fig. 1. Evaluation of the J-integral. (a) General path ABA′CA enclosing a crack tip C. (b) Path ABCDEFGA following the surface of a rectangular electrical fatigue specimen. (c) Path BCDEB enclosing a specimen with a growing damaged zone. (d) Calculation of ΔJ from the charge Q vs. voltage V response of the whole specimen.

given that electrical discharge has been observed within fatigue cracks during cyclic loading (see Section 4). This is consistent with the observation[30] that the measured potential drop across a crack in a ferroelectric is much less than that predicted by assuming an impermeable, insulating medium.

In the set of measurements discussed in this paper, detailed information about the electro-mechanical state at each point on the integration path is not readily available, and a steady state approximation of ΔJ is used. For this interpretation, consider a developing damage zone of finite height, spreading into the material specimen in the x_1 direction, as shown in Fig. 1c. The damaged zone behaves as an inhomogeneity whose mechanical and dielectric behaviour differ from the undamaged bulk. By following the contour of integration around the outer surface ABCDEFA of the specimen shown in Fig. 1c, Eq. (6) becomes

$$\Delta J = \int_{\mathrm{CD+EB}} h^{\mathrm{c}} n_1 \,\mathrm{d}\Gamma \tag{7}$$

In steady state, with purely electrical loading of a specimen of width BC $\gg$ CD, the stress σ_{ij} is zero everywhere on the integration path, whilst D_i is uniform and parallel to the x_3 direction on each of the segments CD and EB. Then, labelling the upstream state on CD by a superscript ‘u’ and the downstream state on EB by a superscript ‘d’, Eq. (7) can be rewritten as

$$\Delta J = \int \Delta D_3^{\mathrm{u}}(V)\,\mathrm{d}V - \int \Delta D_3^{\mathrm{d}}(V)\,\mathrm{d}V \tag{8}$$

where $V = \int_{\mathrm{CD}} - E_3\,\mathrm{d}x_3$ is the voltage on the upper electrode DE. Thus ΔJ can be evaluated if the electric displacement is known as a function of applied voltage both upstream and downstream of the zone of damage growth. In practice, the quantities that are easily measured are V and the total charge ΔQ delivered to the upper electrode. In steady state, let the damage zone advance over a small area δA projected onto the upper electrode. This has the effect of converting a region of material of projected area δA from the upstream state to the downstream state. Consequently, the change in the total charge ΔQ delivered to the upper electrode is $\delta(\Delta Q) = \delta A(\Delta D^{\mathrm{d}} - \Delta D^{\mathrm{u}})$ and the expression for ΔJ reads

$$\Delta J = -\int \frac{(\Delta Q|_{A+\delta A} - \Delta Q|_A)}{\delta A}\,\mathrm{d}V \tag{9}$$

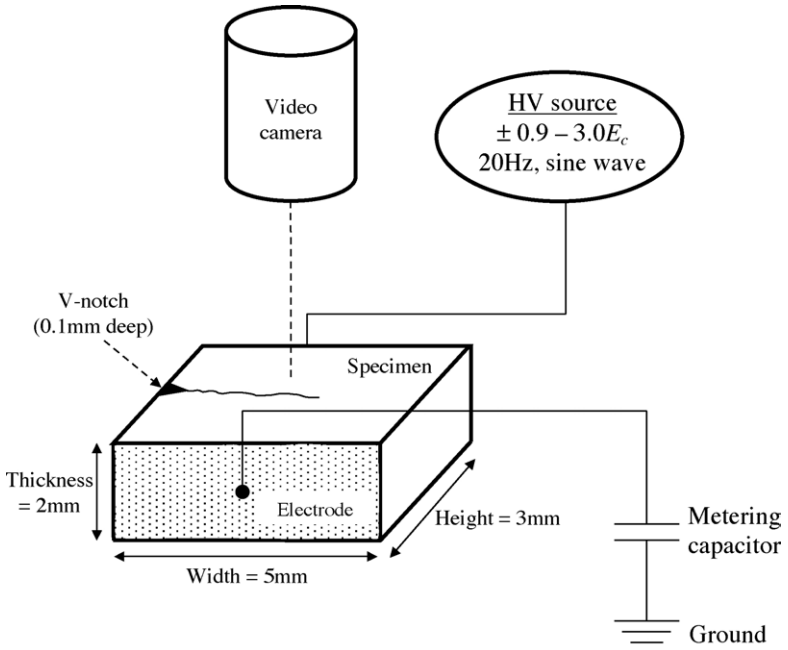

Fig. 2. Schematic of the test specimen and electric field loading apparatus.

as illustrated in Fig. 1d. Eq. (9) is used to estimate the cyclic *J*-integral in this study.

3. Experimental procedure

The general procedures used were as previously reported by Shieh et al.[27] A brief description of the key features of experimental procedure is given here for clarity.

3.1. Choice of materials

The two ceramics PZT-5H and PLZT 8/65/35 were chosen for this study because they are widely used in engineering devices, exhibit nonlinearity at relatively low field strengths, and have strong electromechanical coupling. The PZT-5H was obtained in bulk polycrystalline form[1] with grain size 5–10 μm, a composition close to the morphotropic phase boundary, and a Curie temperature of approximately 195 °C. The PLZT 8/65/35 was also obtained in bulk polycrystalline form,[2] with grain size 3–6 μm, a predominately rhombohedral crystal structure, and a Curie temperature of approximately 110 °C. PLZT 8/65/35 exhibits memory type electro-optical characteristics (birefringence hysteresis). It is transparent in the unpoled and minor-loop states, translucent in the poled ferroelectric state, and birefringent under strain or electric field. Both the PZT-5H and PLZT 8/65/35 materials were thermally depoled to an isotropic state.

3.2. Specimen preparation

Cuboidal specimens measuring 5 mm × 2 mm × 3 mm (width × thickness × height) were cut from the bulk materials. The general arrangement is shown in Fig. 2. Silver-based paints were applied onto the 5 mm × 2 mm faces of the specimens to form electrodes, and all other surfaces were polished to a 1-μm finish. (Unpolished specimens were found to develop numerous cracks rapidly during high amplitude cyclic loading.) A V-notch of depth approximately 0.1 mm was then scribed mid-way between the electrodes on one of the 2 mm × 3 mm side faces with a diamond-tipped scriber; the V-notch was parallel to the electrodes and ran across the entire 2 mm thickness of each specimen. The fatigue cracks were initiated from a notch to produce, as nearly as possible, a through-thickness crack. Conductive epoxy was used to connect wires to the electroded surfaces of the specimens for electric field excitation.

3.3. Equipment and testing

Electric field loading was applied using a high-voltage amplifier, driven by a signal generator. The net charge on the electrodes of each specimen was monitored by a 2.96 μF metering capacitor connected in series between the specimen and ground. From the high voltage source, a bipolar cyclic voltage of sinusoidal waveform at a frequency of 20 Hz was applied to each specimen, to produce electric field parallel to the 3 mm height direction of the specimen. Fully reversed

[1] Morgan Matroc Ltd., Transducer Products Division, Thornhill, Southampton SO9 5QF, UK.
[2] Alpha Ceramics Inc., 5121 Winnetka Avenue North, Minneapolis, MN 55428, USA.

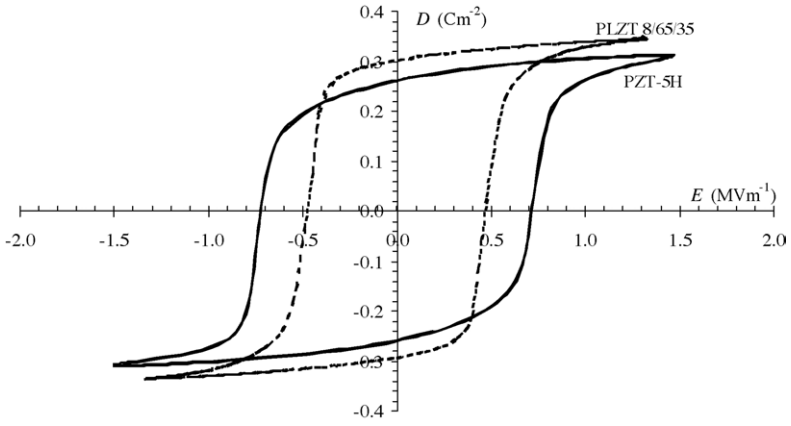

Fig. 3. Measured electric displacement D vs. electric field E hysteresis curves after 10 cycles for PZT-5H and PLZT 8/65/35; loading frequency = 0.2 Hz.

electric loading was applied, with the amplitude of the cyclic field set to selected values in the range $0.9E_c$ to $3.0E_c$ (where E_c is the coercive field of the test material). Electrical breakdown outside the specimen was prevented by immersion in oil, which was filtered regularly to remove any conductive contaminant particles. (Preliminary trials showed that contamination in the oil could contribute to the nucleation of microcracks on the specimen surface.) A long-focal-length video camera was used to observe and record fatigue crack growth and a digital cycle counter was used to track the cycle number. All tests were carried out at laboratory temperatures in the range 17–21 °C. Some temperature rise in the specimen was expected during high amplitude electric field testing due to dissipation associated with ferroelectric switching. Periodic checks were made on the specimen and oil temperature using remote infrared sensing; it was found that the oil temperature in the vicinity of the specimen remained stable and close to the laboratory temperature throughout the tests.

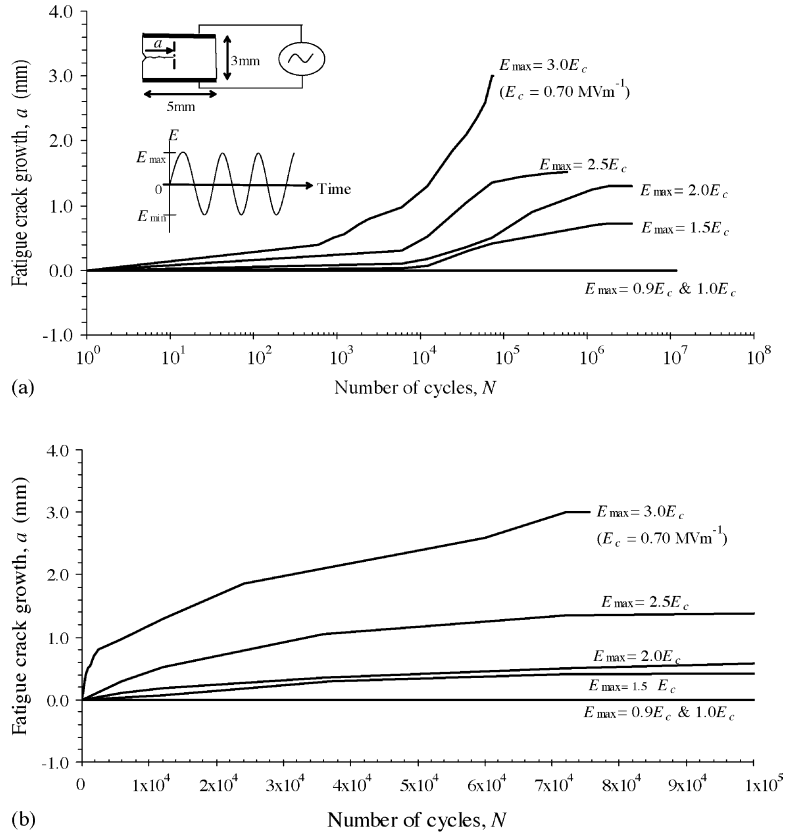

Fig. 4. Comparative a vs. N curves for V-notched PZT-5H, at 20 Hz. (a) Results for the entire test duration, shown on log-linear axes. (b) The first 10^5 cycles of the same tests shown on linear axes.

3.4. Preliminary measurement of hysteresis

The stable cyclic dielectric hysteresis (electric displacement D versus electric field E) of each material was measured before commencing the fatigue tests. A cyclic electric field of amplitude 1.4 MV m^{-1}, frequency of 0.2 Hz, and sinusoidal waveform was applied to an un-notched specimen of each material. The measured D–E curves for PZT-5H and PLZT 8/65/35 are shown in Fig. 3, and the resulting values of coercive field E_c and saturation remanent polarization P_r of both materials are listed in Table 1, along with manufacturers' data for dielectric permittivity K_{33}^T, piezoelectric coefficient d_{33} and Curie temperature T_c.

Table 1
Properties of PZT-5H and PLZT 8/65/35 (K_{33}^T, d_{33} and T_c are manufacturers' data)

Quantity	PZT-5H	PLZT 8/65/35
Coercive field, E_c (MV m^{-1})	0.70	0.48
Remanent polarization, P_r (C m^{-2})	0.26	0.30
Relative dielectric constant, K_{33}^T	3400	3350
Piezoelectric strain coefficient, d_{33} ($\times 10^{-12}$ m V^{-1})	593	640
Curie temperature, T_c (°C)	195	110

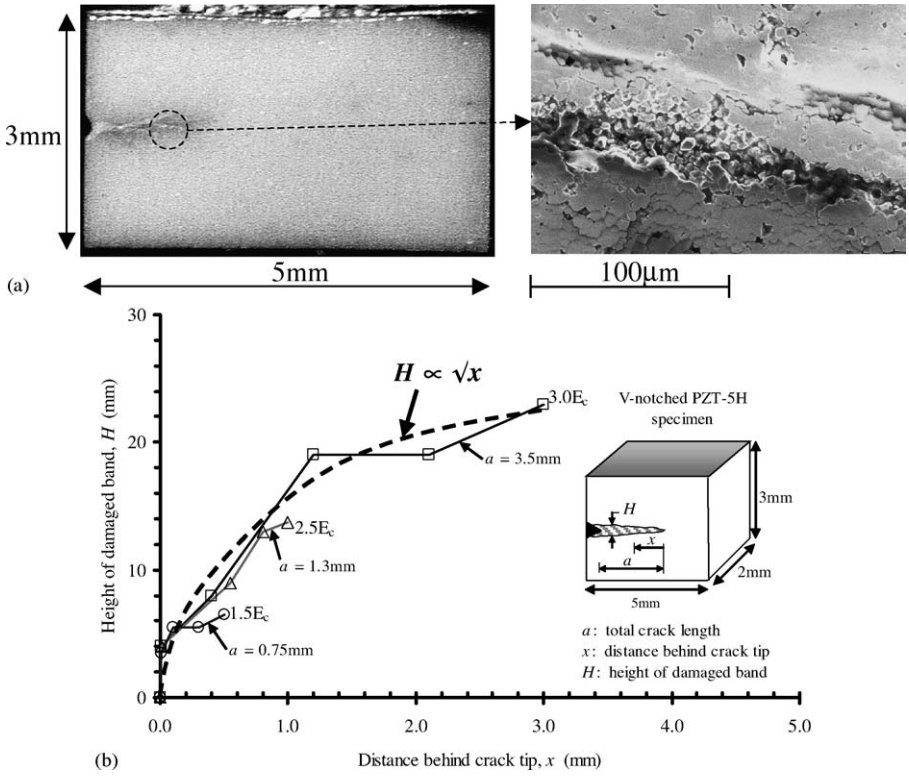

Fig. 5. (a) SEM images of a band of damaged material on crack flanks (PZT-5H). (b) Damaged band height H vs. distance behind the crack tip, x, for specimens loaded at various amplitudes of electric field. All specimens were V-notched PZT-5H; loading frequency = 20 Hz.

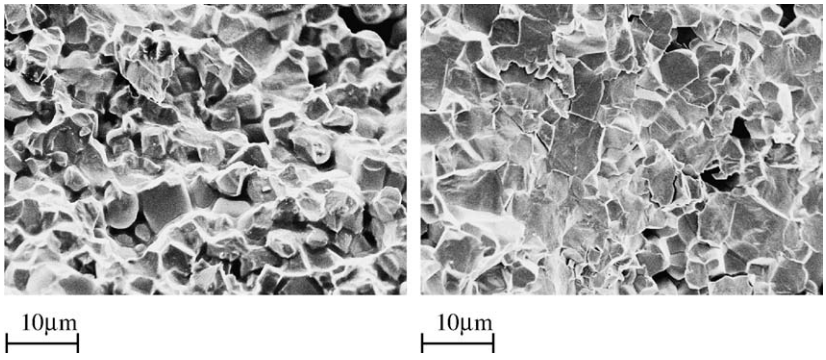

Fig. 6. (a) Electrically fatigue-induced intergranular fracture surface (PZT-5H). (b) Mechanically separated transgranular fracture surface (PZT-5H).

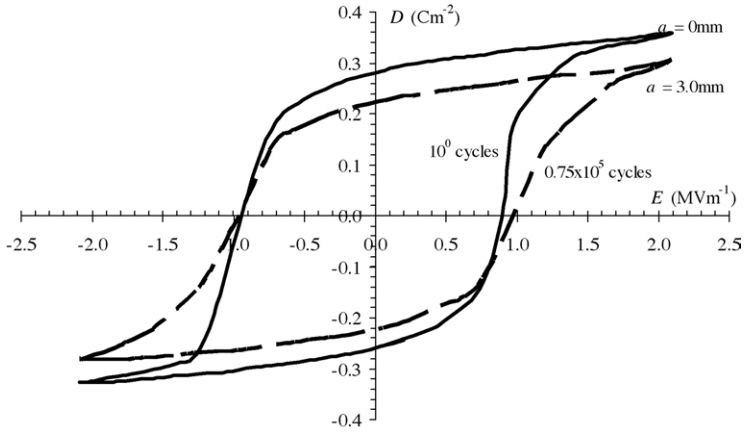

Fig. 7. *D–E* curves at the first cycle and after 0.75×10^5 cycles of loading (arrest of crack growth) in PZT-5H; loading amplitude = $3.0E_c$, loading frequency = 20 Hz.

4. Results and discussion

4.1. Fatigue crack growth in PZT-5H

The crack extension, *a*, as a function of the number of cycles, *N*, under various amplitudes of bipolar electrical loading for the V-notched PZT-5H specimens is shown in Fig. 4a on log-linear axes. In each specimen, crack growth began immediately, with no incubation period. The rate of fatigue crack growth d*a*/d*N* decreased with increasing number of cycles until crack arrest (see Fig. 4b). For the sample loaded to a maximum value $E_{max} = 3.0E_c$, the observation of crack growth was terminated at about 7×10^4 cycles due to the initiation of secondary cracking at the electrodes. Crack arrest occurred after approximately 7×10^4 cycles for the applied field of $E_{max} = 2.5E_c$, and after approximately 2×10^6 cycles

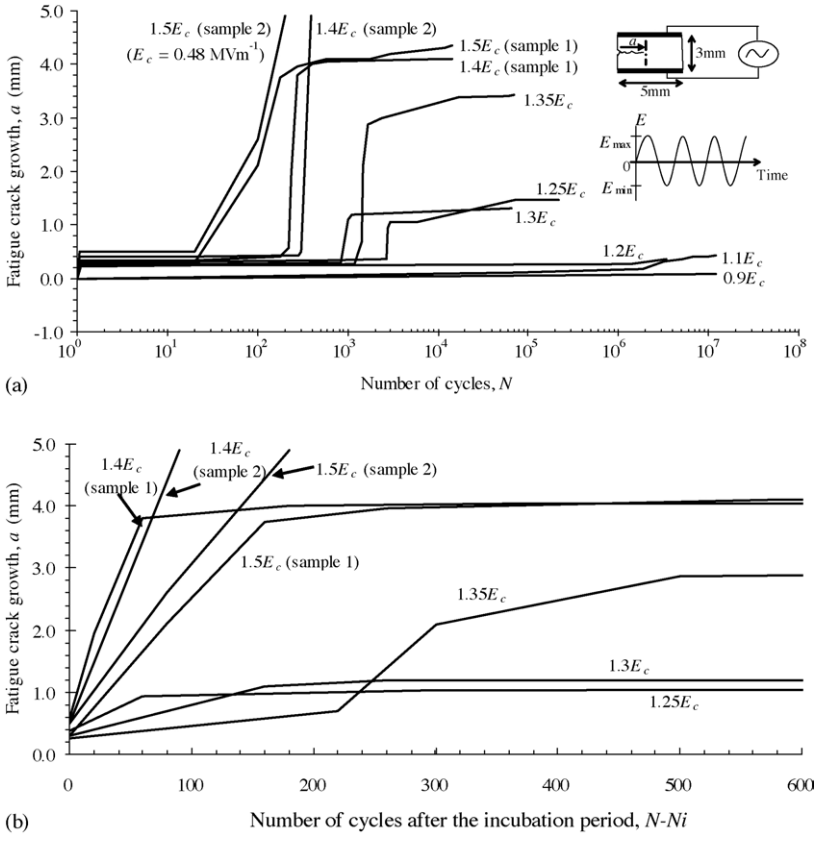

Fig. 8. Comparative *a* vs. *N* curves for V-notched PLZT 8/65/35, at 20 Hz. (a) Results for the entire test duration, on log-linear axes. (b) Results for the first 600 cycles after the incubation period, on linear axes.

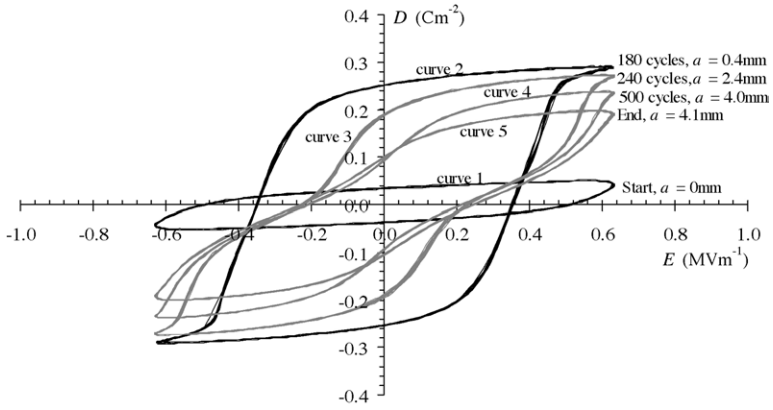

Fig. 9. Progressive change of D–E loop of PLZT 8/65/35 during fatigue testing (load amplitude = $1.4E_c$, sample 1, loading frequency = 20 Hz).

for the applied fields of $E_{max} = 2.0E_c$ and $1.5E_c$. Fatigue crack growth under the alternating electric field of amplitudes $1.0E_c$ and $0.9E_c$ was undetectable by the video imaging system after 10^7 cycles. Both the arrested fatigue crack length and the average crack growth rate increased with electric field amplitude in PZT-5H. Here, the average crack growth rate is defined by the total crack extension to crack arrest divided by the total number of cycles to crack arrest.

The fatigue cracks in PZT-5H were observed to emanate from the tip of the V-notch. Some crack branching was observed, but the predominant direction of crack growth was along the mid-plane of the specimen perpendicular to the applied electric field. With nominal field amplitudes above $2.0E_c$, electrical arcing was clearly visible within the fatigue crack during the tests. As the fatigue crack propagated through the ceramic, a band of damaged material formed around the crack (see Fig. 5a) and later examination of the specimen surface by scanning electron microscopy (SEM) indicated fragmentation into discrete grains along the crack flanks. The height H of the damage band is plotted as a function of distance x behind the crack tip in Fig. 5b for selected values of E_{max}. It is evident that H varies approximately with $x^{1/2}$ and is independent of load level. This behaviour is characteristic of the near crack-tip region of a crack-like

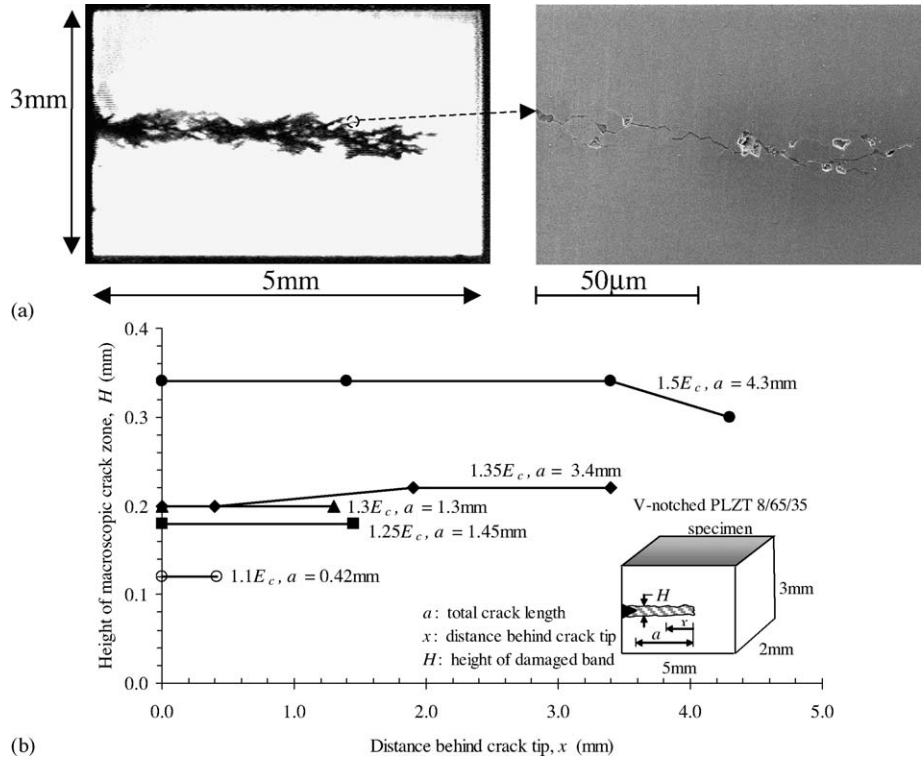

Fig. 10. (a) The development of a single macroscopic zone of microcracks in V-notched PLZT 8/65/35 specimen after 1.44×10^4 cycles at $1.5E_c$, 20 Hz. (b) Cracking zone height vs. distance behind crack tip at various applied electric fields for V-notched PLZT 8/65/35; loading frequency = 20 Hz.

feature propagating in steady state. After fatigue testing, the specimens were broken open by applying a mechanical load until separation occurred, through the fatigue crack growth zone. Examination of the fracture surfaces by SEM indicated that the fatigue crack in the PZT-5H specimen existed across the section thickness and was not merely a superficial crack. The fatigue-crack surface was predominantly intergranular, whereas the monotonic fracture surface under tensile loading was predominantly transgranular (compare Fig. 6a and b). Micro-cracks, wear debris and pulverised material were apparent on the fatigue-induced intergranular fracture surfaces, giving the appearance of severe wear.

The evolution of the nominal *D–E* curves for the $E_{max} = 3.0E_c$ specimen, from that recorded at the start of the fatigue loading to that after crack arrest ($a = 3$ mm), is shown in Fig. 7. A 15% reduction in the saturation remanent polarization of the specimen was observed during the test, and the switch of polarisation in the vicinity of the coercive field strength became less abrupt with increased cycling.

4.2. Fatigue crack growth in PLZT 8/65/35

The PLZT 8/65/35 ceramic also showed crack growth and arrest under a fully reversed cyclic electric field. The fatigue crack extension, a, is shown in Fig. 8a as a function of the number of cycles, N, at selected amplitudes of bipolar electrical loading. At field amplitudes below $1.2E_c$, fatigue crack growth was negligible. At greater amplitudes, cracks grew until they arrested at a crack length which increased with load amplitude. When the field amplitude was greater than $1.2E_c$, three distinct stages were observed: an incubation period of N_i cycles, during which crack growth was negligible, a period of rapid crack growth, and finally, crack arrest. The number of cycles N_i in the incubation period reduced monotonically with increasing electric field amplitude. The rapid, steady growth rate after the incubation period was about 10–40 μm/cycle for all specimens, with some sensitivity to E_{max}. Fig. 8b shows the crack growth after the incubation period for each specimen, on log-linear scales.

A progressive change in shape of the nominal *D–E* hysteresis curve during fully reversed cyclic loading was observed in all of the specimens. Fig. 9 shows this progression for the specimen loaded at amplitude $E_{max} = 1.4E_c$ (labelled sample 1 at $1.4E_c$ in Fig. 8). At the start of the fatigue test (curve 1 in Fig. 9) the *D–E* curve was a minor-loop with little ferroelectric switching; this corresponded to the incubation period of 180 cycles shown in Fig. 8a. At approximately 180 cycles, the *D–E* curve expanded into a major-loop (see curve 2 in Fig. 9), corresponding to the onset of rapid fatigue crack growth at about 50 μm/cycle. During the period of rapid growth, the *D–E* curve collapsed gradually from the major-loop state (see curve 3 in Fig. 9) until, at about 500

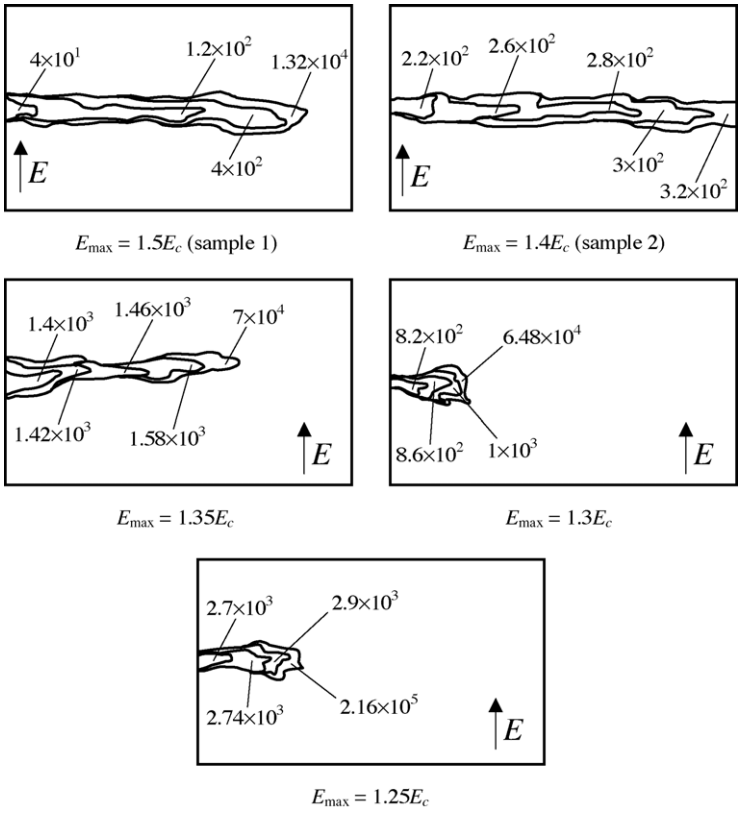

Fig. 11. Evolution of the cracked zone with cycle number in various V-notched PLZT 8/65/35 specimens. Heavy contours show the extent of the damage zone at the number of cycles indicated.

cycles, fatigue crack growth arrested. During the following 10^4 cycles, there was little crack growth, and only a slight change in the *D–E* curve. The *D–E* curves for specimens cycled at and below $1.2E_c$ stayed in the minor-loop (low hysteresis) state throughout the test—these specimens showed negligible crack growth.

Fatigue crack growth in PLZT 8/65/35 was by the development of a single macroscopic zone of microcracks which exhibited features such as bifurcation and tunnelling (see Fig. 10a). The microcracked zone had an approximately constant height along its entire length. However, the zone height increased monotonically with the strength of the applied electric field — ranging from about 0.12 mm for a field strength of $E_{max} = 1.1E_c$ to about 0.35 mm for $E_{max} = 1.5E_c$ (see Fig. 10b). Subsequent SEM inspection of sectioned specimens and fracture surfaces showed that the microcracks were isolated intergranular cracks. This suggests that the microcracks form by the failure of grain boundaries due to local conditions in the vicinity of the individual grains. Since PLZT 8/65/35 is transparent, it was possible to observe that the zone bifurcated severely and was not continuous through the whole thickness of the specimen. Electrical arcing within the microcracked zone during high amplitude testing was also visible in PLZT 8/65/35.

The evolution of the length and shape of the microcracked zone with fatigue cycles for various PLZT 8/65/35 specimens is shown on a side view of the specimen in Fig. 11: the contours give the boundary of the microcracked zone with increasing number of cycles. For each specimen, a gradual broadening of the macroscopic zone of microcracks in the direction of the applied electric field is observed, whilst the predominant direction growth was along the centreline of the specimen, perpendicular to the applied electric field.

4.3. Dielectric hysteresis of microcracked material and uncracked material

Measurements of the dielectric response of uncracked material and material taken from the microcracked zone were made, as follows. A V-notched PLZT 8/65/35 specimen was subjected to a cyclic electric field of $E_{max} = 1.4E_c$ at 20 Hz, until the macroscopic zone of microcracks grew across the full width of the specimen. The uncracked and microcracked regions of the fatigued V-notched specimen were then cut out as separate specimens, with dimensions

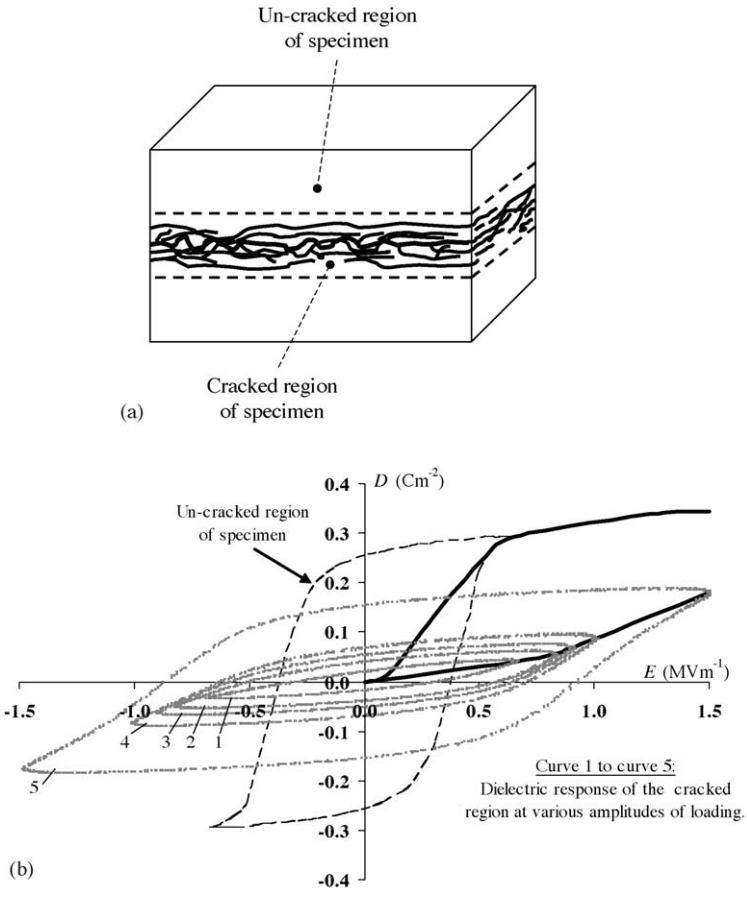

Fig. 12. (a) The un-cracked and cracked regions of the fatigued PLZT 8/65/35 specimen are cut out as two separated specimens. (b) Measured *D–E* responses for cracked and uncracked regions of the fatigued PLZT 8/65/35 specimen; loading frequency = 20 Hz. The bold lines link the tips of the hysteresis loops for both the uncracked and the cracked material.

5 mm × 2 mm × 0.5 mm (see Fig. 12a). Silver paint was applied onto the 5 mm × 2 mm faces of these specimens to form electrodes, and the resulting specimens were subjected to cyclic electrical loading whilst surface charge was measured, using the arrangement shown in Fig. 2.

Fig. 12b shows the nominal *D–E* curves of the uncracked and microcracked material specimens, measured at 20 Hz. The *D–E* response of the uncracked region was similar to that of the whole specimen, measured early in the fatigue test, but after the incubation period (compare Fig. 9, curve 2). This indicates that the dielectric behaviour of the uncracked region is almost unchanged by the fatigue process. However, the microcracked region showed a reduced amplitude of electric displacement and an increased coercive field. Curves 1–5 in Fig. 12b show the stable cyclic *D–E* response of the microcracked region cycled at various electric field amplitudes, in the range 0.67 MV m^{-1} to 1.5 MV m^{-1}. It is evident that the cracked region of the fatigued PLZT 8/65/35 specimen behaves as a dielectric inhomogeneity. Continuity of electric displacement throughout the fatigue specimens requires most of the drop in electric potential to be across the microcracked zone. Thus the microcracked zone produces a local enhancement of electric field, that influences switching in nearby grains. The bold lines in Fig. 12b show the locus of the tips of the *D–E* hysteresis loops for both microcracked and uncracked material.

4.4. Influence of specimen geometry

In order to investigate the effects of specimen geometry on the morphology of the microcracked zone, PLZT 8/65/35 specimens with increased width (10 mm × 3 mm × 2 mm) and with increased height (5 mm × 12 mm × 2 mm) were prepared. These specimens were first V-notched and electroded, and were then subjected to loading with a fully reversed cyclic electric field of amplitude 1.5E_c. This provides a direct comparison with the 5 mm × 3 mm × 2 mm specimens subjected to the same amplitude of loading. The cyclic loading was continued until crack growth arrested, or reached the specimen surface opposite the V-notch. Images of each specimen taken at test completion, using the video imaging system, are shown in Fig. 13a. The height of the microcracked zone increased with both specimen height and width. In the 10 mm × 3 mm × 2 mm specimen, a gradual increase of height of the microcracked zone across the specimen width was observed. The length of the microcracked zone *a* versus the number of loading cycles *N* is shown in Fig. 13b, which shows a significantly longer incubation period for the specimens with increased width and height.

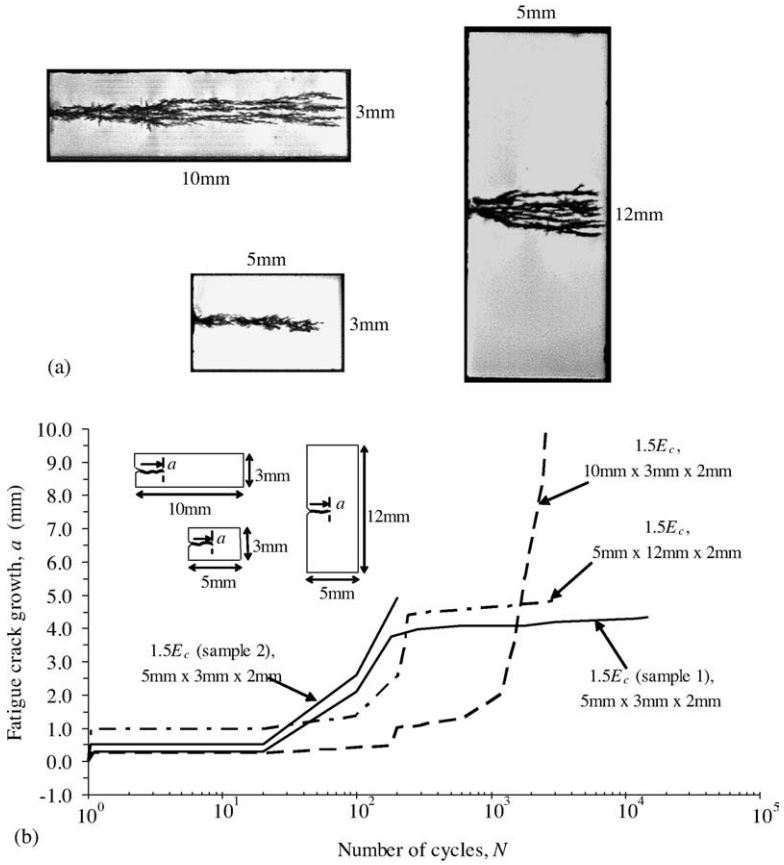

Fig. 13. Fatigue damage zone growth in PLZT 8/65/35 for specimens of various geometries. (a) Images of the specimens after fatigue testing. (b) Fatigue damage zone growth, *a*, vs. number of cycles *N*.

4.5. The search for a correlating parameter

The fatigue crack growth data (a versus N) shown in Fig. 4 for PZT-5H and Fig. 8 for PLZT 8/65/35 exhibit changes in growth rate da/dN which correlate with qualitative changes in the cyclic hysteresis (D versus E) of the specimen, as discussed in Sections 4.1 and 4.2. Note that da/dN does not increase monotonically with a at constant load amplitude, as would be expected if the electric field intensity range ΔK_{E} controlled the growth rate. A quantitative comparison with various potential correlating parameters is made by plotting da/dN against trial correlating parameters, to determine which parameter best collapses the data to a simple relationship. The parameters considered here are: the range of applied electric field, ΔE; the range of applied voltage, ΔV; the range of electric displacement, ΔD; the cyclic J-integral, ΔJ; and the cyclic dissipation, ΔW. The value of ΔE used is the volume average, given by $\Delta V/H_{\mathrm{s}}$, where H_{s} is the specimen height. Similarly ΔD is the nominal value, calculated by dividing the peak to peak change in charge on a surface electrode by the electrode area A. The values of ΔJ are estimates evaluated by using Eq. (9). The cyclic dissipation ΔW is calculated by $\Delta W = \oint(Q\,\mathrm{d}V/AH_{\mathrm{s}})$ where the integration is carried out over one full cycle of loading. This quantity is the volumetric dissipation of electrical energy in each cycle; the energy is potentially available for the bulk degradation processes characteristic of electrical fatigue.

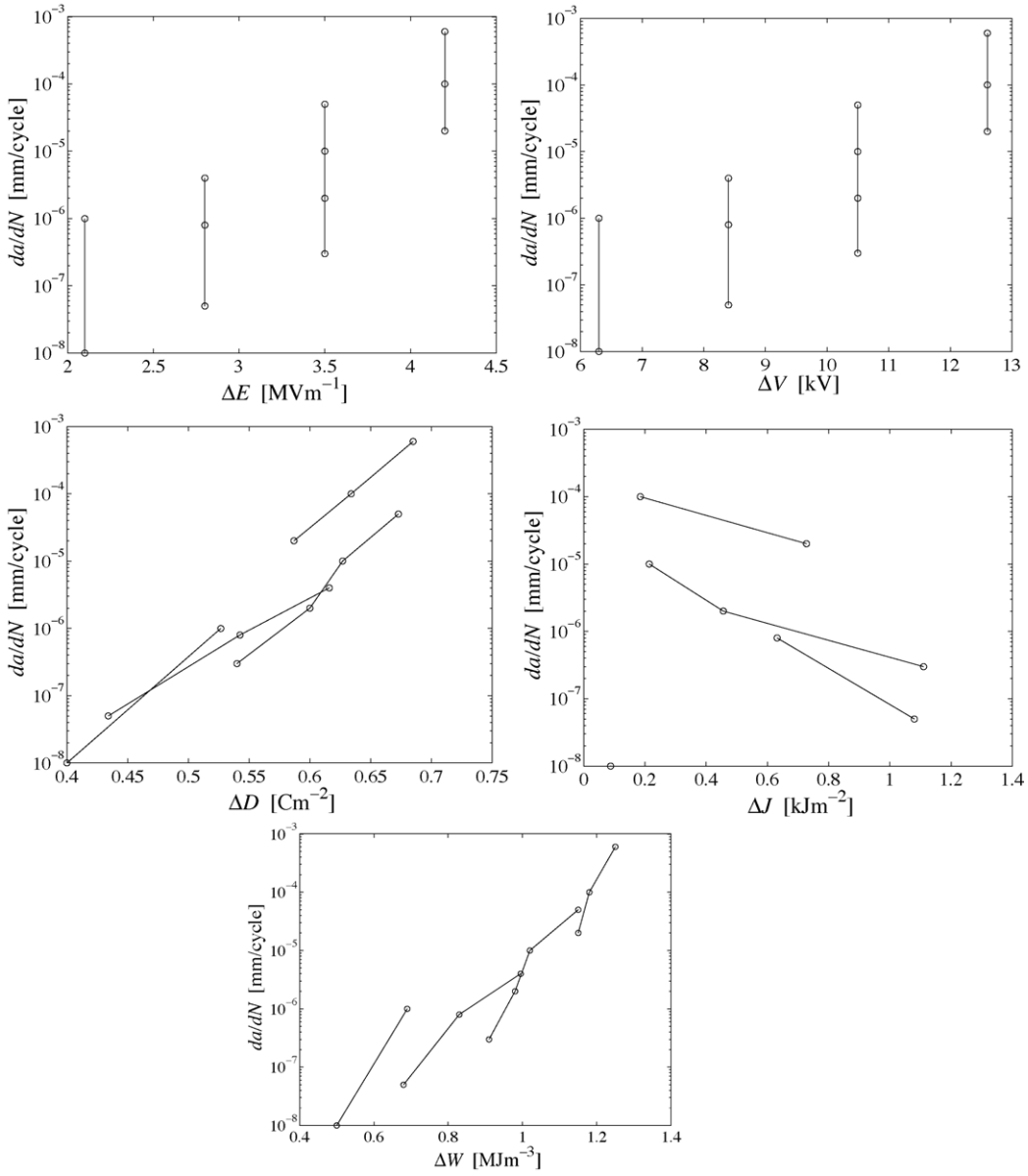

Fig. 14. (a) Fatigue crack growth rate (da/dN) vs. potential correlating parameters (ΔE, ΔV, ΔD, ΔJ and ΔW) for various PZT-5H specimens. (b) Fatigue crack growth rate (da/dN) vs. potential correlating parameters (ΔE, ΔV, ΔD, ΔJ and ΔW) for various PLZT 8/65/35 specimens.

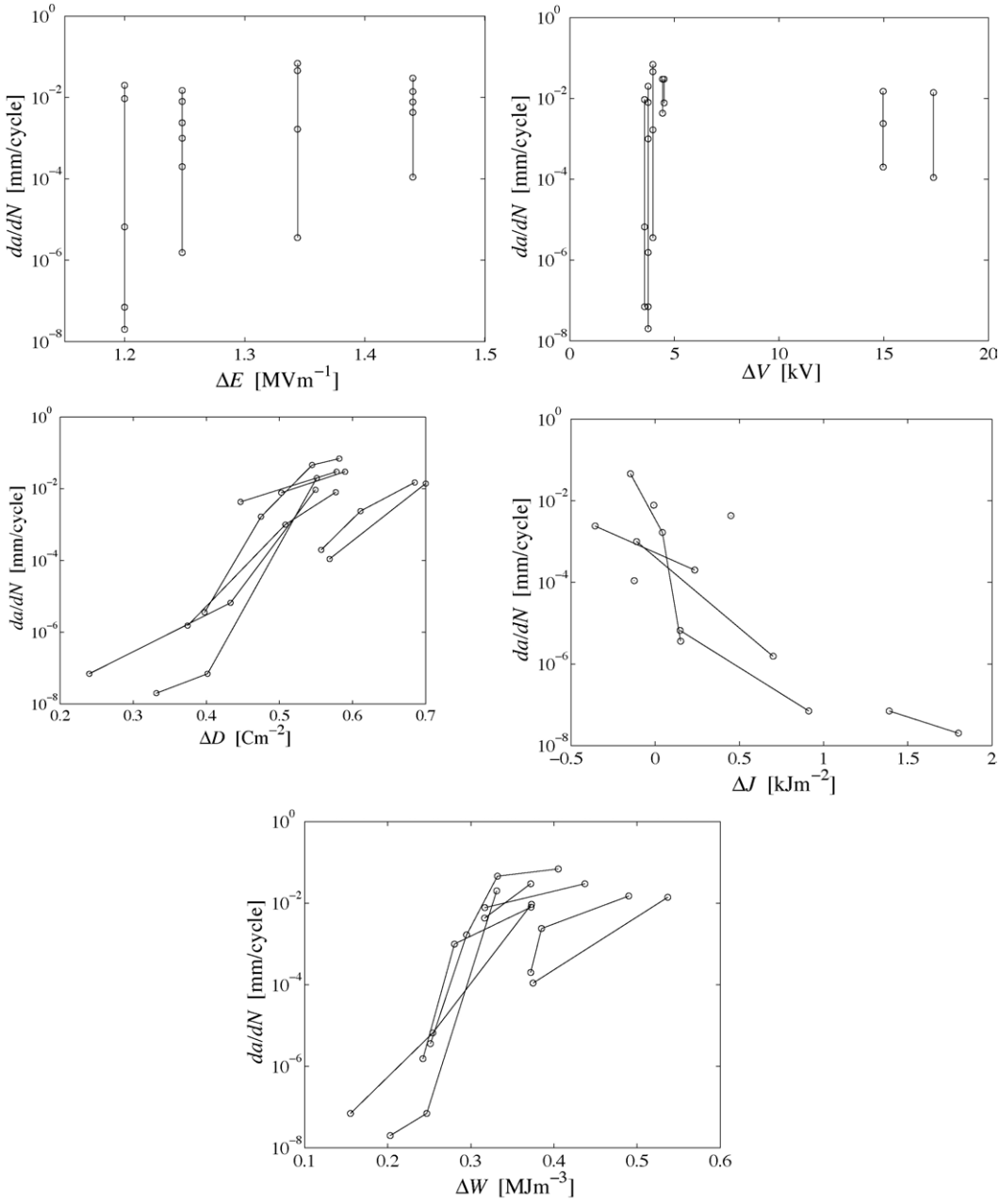

Fig. 14. (*Continued*).

The growth rate da/dN is plotted against each correlating parameter for PZT-5H and PLZT 8/65/35 in Fig. 14a and b, using log-linear axes. In each case, solid lines link data points taken from the same specimen; the individual data points refer to the points within each test at which the correlating parameters were evaluated. Since da/dN varied during each test, an evaluation of da/dN and each of the correlating parameters was made at several points during each test. Where possible, an evaluation was made during the initial stage of the test (before rapid growth), one or more evaluations were made during the rapid growth stage, and an evaluation was made at or near the arrest stage. Note, however, that these stages were not always present, nor clearly distinct. For simplicity, the relation of the individual points to the stages of each test is not indicated in Fig. 14. A correlation is sought between each parameter and da/dN, which is independent of the particular test or stage.

Fig. 14 shows the strong sensitivity of da/dN to the loading level: changes in any of the correlating parameters of less than one order result in several orders of magnitude change in growth rate. Although there is a trend towards increasing da/dN with increasing ΔE or ΔV, there is no strong correlation between either of these parameters and da/dN across all the measurements. This is a direct result of the large range of da/dN observed during individual tests (at fixed ΔE and ΔV). There is, however, a fairly good correlation between

growth rate and ΔD in both materials, suggesting a relationship of the form $da/dN = A_0 e^{(\Delta D/D_0)}$ in the loading range $E_{max} = 0.9E_c$ to $3.0E_c$, with A_0 and D_0 treated as material constants. The scatter of results is such that a power law relationship cannot be ruled out. A moderately good correlation with ΔW is also seen in Fig. 14. Note that, to within a factor of order unity, ΔW is given by $\Delta E\,\Delta D$. There is a poor correlation of growth rate with the estimate of ΔJ in both materials.

5. Conclusions

Fatigue crack growth data have been presented for two ferroelectric materials, PZT-5H and PLZT 8/65/35, subjected to purely electrical loading. Under fully reversed cyclic loading with amplitude $E_{max} = 0.9E_c$ to $3.0E_c$, cracks grow from a V-notch in both materials, with the predominant direction of growth perpendicular to the applied electric field. An initial incubation period is observed in PLZT 8/65/35 but not in PZT-5H. In both materials, the rate of advance of cracks decreases with increasing cycle number, finally resulting in arrest. The arrested crack length Δa_{arrest} increases with loading amplitude E_{max}. For the case of PZT-5H a damaged band of material forms, consisting of separated grains, with the height of the band varying parabolically with distance from the crack tip. In contrast, in PLZT 8/65/35, a zone of microcracked material of almost uniform height spreads across the material. The rate of advance of the cracks correlates reasonably well with the nominal electric displacement amplitude ΔD, calculated by dividing the peak to peak change in charge on a surface electrode by the electrode area. The correlation appears exponential in the loading regime considered, but there is a broad scatter in the data. Further study is needed to clarify the electro-mechanical source of fatigue cracking and to understand the arrest process. The damage growth rate correlates neither with electric field amplitude ΔE, nor with the cyclic J-integral ΔJ, suggesting that a local damage mechanics approach may be more appropriate than field intensity or energy release rate for modelling this phenomenon. Since the cracked zone of material acts as a dielectric inhomogeneity, it produces a region of enhanced electric field ahead of it, where individual grain boundaries have an increased probability of failure. This suggests that crack advance or arrest is a stochastic process depending on local heterogeneity of switching behaviour and on the distribution of grain boundary flaws.

Acknowledgements

The authors are grateful to Q. Liu for providing separate measurements of hysteresis in PLZT 8/65/35 which have helped in preparing Fig. 12b. JEH is supported by the Royal Society under the University Research Fellowship scheme.

References

1. Moulson, A. J. and Herbert, J. M., *Electroceramics: Materials, Properties, and Applications*. Chapman & Hall, London, 1990.
2. Xu, Y., *Ferroelectric Materials and Their Applications*. North Holland, Amsterdam, 1991.
3. Okazaki, K. and Tanimoto, T., Electro-mechanical strength and fatigue of ferroelectric ceramics. *Ferroelectrics*, 1992, **131**, 25–40.
4. Lynch, C. S., Chen, L., Yang, W., Suo, Z. and McMeeking, R. M., Crack growth in ferroelectric ceramics driven by cyclic polarization switching. *J. Intell. Mater. Syst. Struct.*, 1995, **6**(2), 191–198.
5. Schneider, G. A. and Heyer, V., Influence of the electric field on Vickers indentation crack growth in $BaTiO_3$. *J. Eur. Ceram. Soc.*, 1999, **19**, 1299–1306.
6. Cao, H. and Evans, A. G., Electric-field-induced fatigue crack growth in piezoelectrics. *J. Am. Ceram. Soc.*, 1994, **77**(7), 1783–1786.
7. Zhu, T., Fang, F. and Yang, W., Fatigue crack growth in ferroelectric ceramics below the coercive field. *J. Mater. Sci. Lett.*, 1999, **18**, 1025–1027.
8. Weitzing, H., Schneider, G. A., Steffens, J., Hammer, M. and Hoffmann, M. J., Cyclic fatigue due to electric loading in ferroelectric ceramics. *J. Eur. Ceram. Soc.*, 1999, **19**, 1333–1337.
9. Fang, F., Yang, W. and Zhu, T., Crack tip 90° domain switching in tetragonal lanthanum-modified lead zirconate titanate under an electric field. *J. Mater. Res.*, 1999, **14**(7), 2940–2944.
10. Yang, W., Fang, F. and Zhu, T., Microscopic deformation at a crack tip in a ferroelectric material. *Key Eng. Mater.*, 2000, **183–187**, 175–180.
11. Xu, Z., Tan, X., Han, P. and Shang, J. K., In situ transmission electron microscopy study of electric-field-induced microcracking in single crystal $Pb(Mg_{1/3}Nb_{2/3})O_3$-$PbTiO_3$. *Appl. Phys. Lett.*, 2000, **76**(25), 3732–3734.
12. Tan, X. and Shang, J. K., Crack deflection in relaxor ferroelectric PLZT under inclined cyclic electric field. *Scripta Materialia*, 2000, **43**, 925–928.
13. Shang, J. K. and Tan, X., A maximum strain criterion for electric-field-induced fatigue crack propagation in ferroelectric ceramics. *Mater. Sci. Eng.*, 2001, **A301**, 131–139.
14. Zhu, T. and Yang, W., Toughness variation of ferroelectrics by polarization switch under non-uniform electric field. *Acta Mater.*, 1997, **45**(11), 4695–4702.
15. Yang, W. and Zhu, T., Switch-toughening of ferroelectrics subjected to electric fields. *J. Mech. Phys. Solids*, 1998, **46**, 291–311.
16. Yang, W. and Zhu, T., Fracture and fatigue of ferroelectrics under electric and mechanical loading. *Fatigue Fracture Eng. Mater. Struct.*, 1998, **21**, 1361–1369.
17. Zhu, T. and Yang, W., Fatigue crack growth in ferroelectrics driven by cyclic electric loading. *J. Mech. Phys. Solids*, 1999, **47**, 81–97.
18. Jiang, Q., Cao, W. and Cross, L. E., Electric fatigue in lead zirconate titanate ceramics. *J. Am. Ceram. Soc.*, 1994, **77**(1), 211–215.
19. White, G. S., Raynes, A. S., Vaudin, M. D. and Freiman, S. W., Fracture-behavior of cyclically loaded PZT. *J. Am. Ceram. Soc.*, 1994, **77**(10), 2603–2608.
20. Dausch, D. E., Ferroelectric polarization fatigue in PZT-based RAINBOWs and bulk ceramics. *J. Am. Ceram. Soc.*, 1997, **80**(9), 2355–2360.
21. Levstik, A., Filipic, C., Bobnar, V. and Kosec, M., Electric field induced cracking in PLZT ceramics. *Ferroelectrics*, 1997, **201**, 263–268.
22. Wang, D., Fotinich, Y. and Carman, G. P., Influence of temperature on the electromechanical and fatigue behavior of piezoelectric ceramics. *J. Appl. Phys.*, 1998, **83**(10), 5342–5350.
23. Qian, R., Lukasiewicz, S. and Gao, Q., Electrical fatigue response for ferroelectric ceramics under electrical cyclic load. *Solid-State Electron.*, 2000, **44**, 1717–1722.
24. Takemura, K., Ozgul, M., Bornand, V., Trolier-McKinstry, S. and Randall, C. A., Fatigue anisotropy in single crystal $Pb(Zn_{1/3}Nb_{2/3})O_3$-$PbTiO_3$. *J. Appl. Phys.*, 2000, **88**(12), 7272–7277.

25. Nuffer, J., Lupascu, D. C. and Rödel, J., Damage evolution in ferroelectric PZT induced by bipolar electric cycling. *Acta Materialia*, 2000, **48**, 3783–3794.
26. Shur, V. Y., Rumyantsev, E., Nikolaeva, E., Shishkin, E., Baturin, I., Shur, A. *et al.*, Kinetics of fatigue in bulk ferroelectrics. *Proc. SPIE*, 2002, **4699**, 40–50.
27. Shieh, J., Fleck, N. A. and Huber, J. E., Observations of fatigue crack growth in ferroelectrics under electrical loading. *Proc. SPIE*, 2002, **4699**, 51–63.
28. Cherepanov, G. P., *Mechanics of Brittle Fracture*. McGraw-Hill, 1979, p. 325.
29. Suresh S, *Fatigue of Materials* (*2nd ed.*). Cambridge, 1998.
30. Schneider, G. A., Felten, F. and McMeeking, R. M., The electrical potential difference across cracks in PZT measured by Kelvin Probe Microscopy and the implications for fracture. *Acta Materialia*, 2003, **51**, 2235–2241.